ACS Partner Journal
CHEM & BIO ENGINEERING

pubs.acs.org/ChemBioEng
Article

Relative Aromaticity/Aliphaticity Steered Pore Structure in Polyamide-Derived Ultramicroporous Carbons for Efficient C_3H_6/C_3H_8 Separation

Published as part of Chem & Bio Engineering virtual special issue "Advanced Separation Materials and Processes".

Abdul Waqas Anjum, Lin Zhu, Jiawu Huang, Neng Liao, Shengjun Du, Zhong Li, Cuiting Yang,* and Jing Xiao*

Cite This: *Chem Bio Eng.* 2024, 1, 960−969

Read Online

ACCESS | Metrics & More | Article Recommendations | Supporting Information

ABSTRACT: Carbon molecular sieves (CMS) with a tunable pore structure hold significant promise for efficient C_3H_6/C_3H_8 separation. However, understanding the relationship between a precursor's carbon framework and the microstructure of carbonized products is still ambiguous and requires further investigation. Herein, a relative aliphaticity/aromaticity regulated strategy was proposed to tailor the carbon skeleton of the polyamide precursor, aiming to fine tune the CMS pore size between the kinetic diameter of C_3H_6 (4.68 Å) and C_3H_8 (5.11 Å). The relative aliphaticity/aromaticity of the precursor was rationally modulated by replacing aromatic rings in diamine monomers with aliphatic chains of different lengths. Results indicated that polyamide precursors with higher relative aliphaticity exhibited increased susceptibility to fragmentation during carbonization. Thus, a higher degree of carbon layer restructuring arising from the degradation of aliphatic chains promoted the formation of orderly graphitized structures with sub 5 Å ultramicropores. The ETDA-derived CMS pyrolyzed at 700 °C (ETDA700) exhibited outstanding sieving performance in separating C_3H_6 from C_3H_8, with C_3H_6 uptakes of up to 2.33 mmol/g, while propane adsorption capacity was negligible. This work may provide valuable insights for the design of sieving carbonaceous material by rationally tuning precursor properties for the efficient separation of gas mixtures with similar sizes.

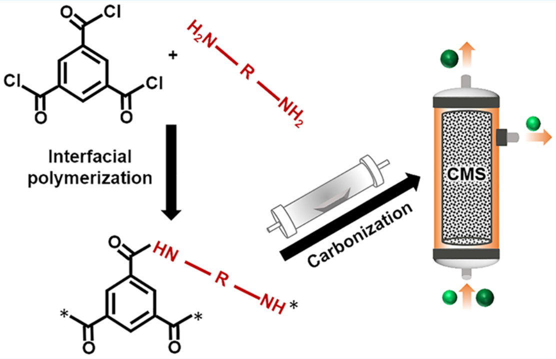

KEYWORDS: *adsorption, C_3H_6/C_3H_8 separation, pore structure, size-sieving, carbon*

1. INTRODUCTION

Propylene (C_3H_6) is an important industrial raw material in the synthesis of commercially high-value chemicals such as polypropylene, propylene oxide, propylene glycol, acrylonitrile, cumene, and polyols.[1] The global demand for propylene is expected to reach 1.3 billion tons by 2025, growing persistently at 4−5% per annum.[2] However, propylene is mainly manufactured via steam cracking in a mixture with propane,[3] posing great difficulties in the subsequent separation due to their similar physicochemical properties (boiling point, 225 K for C_3H_6 and 231 K for C_3H_8; kinetic diameter, 4.67 Å for C_3H_6 and 5.11 Å for C_3H_8).[4] Adsorption separation is emerging as a potential alternative to the traditional energy-intense cryogenic distillation for the C_3H_6/C_3H_8 separation, where advanced adsorbents are essential.[5] Carbon molecular sieves (CMS), a special type of carbonaceous materials with the advantages of narrow pore size distribution enabling the separation of small molecules through the size-sieving effect, along with high stability and easy availability, have attracted wide attention in the field of gas separation and have been successfully applied in the separation of CO_2/N_2,[6] CO_2/CH_4,[7] CH_4/N_2,[8] C_2H_4/C_2H_6,[9] and C_3H_6/C_3H_8.[10]

Carbonization of polymeric precursors is a representative method for CMS synthesis, which involves the transformation of precursors into amorphous carbon networks incorporating abundant ultramicropores, which serve as permeation channels for gas separation. Since the carbonization of precursors involves intricate reactions between different functional groups present within the polymeric backbone, the structural proper-

Received: April 30, 2024
Revised: July 18, 2024
Accepted: July 18, 2024
Published: July 31, 2024

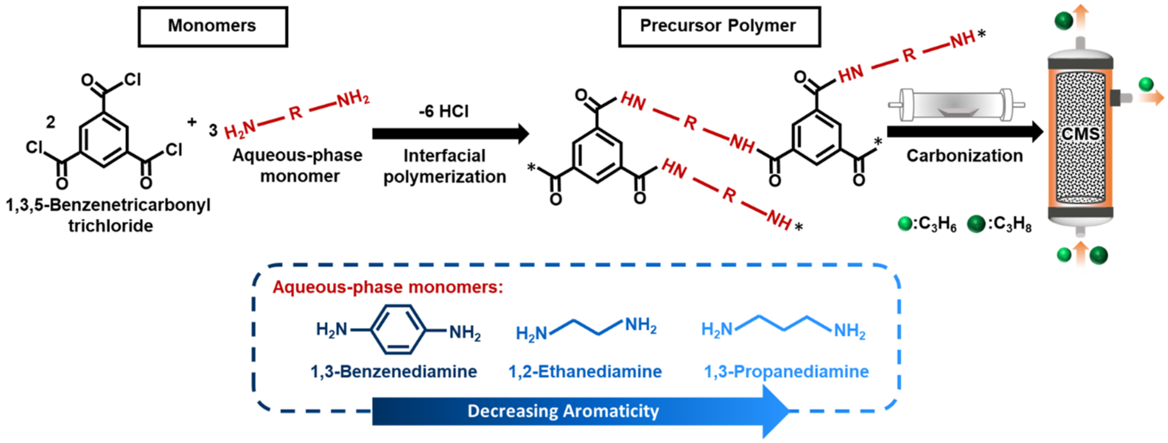

Figure 1. Synthesis of precursor polyamides through interfacial polymerization of 1,3,5-benzenetricarbonyl trichloride with different diamine monomers to vary the relative aromaticity followed by carbonization at 700 °C under N_2 to obtain carbon molecular sieves for C_3H_6/C_3H_8 separation.

ties of the precursor have a great effect on the pore architecture and ultimately gas separation performance of CMS.[11] Various studies have been conducted to investigate the impact of different functional groups on the structural properties of carbons. For instance, Babu et al. studied the influence of N-doping on the adsorption characteristics in carbon nanomaterials and compared them with oxygen functionalized carbons.[12] On the other hand, Rahimi et al. evaluated the performance of carbon-based adsorbents, focusing on how variations in oxygen content in the carbon structure influence gas separation characteristics.[13] Also, Kiyono et al. investigated the effect of polymer precursors on the development of carbon molecular sieves and their implications for gas separation performance, emphasizing the role of oxygen in enhancing selective separation.[14] Since these studies have focused on investigating the effects of nitrogen or oxygen only, the role of different carbons, which are present within the precursor framework, has not been studied yet. Specifically, aromaticity, i.e., the presence of a planar, cyclic structure with delocalized π-electrons, is of fundamental importance for organic compounds in defining their stability and reactivity.[15] Contrarily, the absence of resonance stabilization in non-aromatic counterparts leads to higher energy levels, making them less resistant to scission and decomposition during carbonization at high temperatures. Understanding the structure−activity relationship between the relative aromaticity/aliphaticity of the polymeric precursor and the resulting microstructure and gas separation performance of derived CMS not only contributes to elucidating the degradation mechanisms at high temperatures but also facilitates precise control of pore architecture in CMS for gas sieving applications.

Herein, an aromaticity/aliphaticity-driven pore-engineering approach was introduced to precisely regulate the ultramicropore size within sub 5 Å of the CMS for C_3H_6/C_3H_8 separation. The relative aliphaticity/aromaticity of the precursor was adjusted by substituting the aromatic ring of diamines with aliphatic carbons of varying chain lengths in polyamide precursors (Figure 1). The effect of the relative aliphaticity/aromaticity of the precursor on the structural evolution and separation performance of the derived CMS were investigated systematically. Characterization results, including TG-MS, XPS, Raman, etc., combined with multiple probe gases analysis indicated that polyamide precursors containing higher aliphatic content were more readily broken down at low temperature due to the unstable carbon chains, leading to a higher degree of carbon structure rearrangement under less energy input, thus promoting the formation of a more graphitic carbonaceous structure and the creation of smaller structural voids within the carbon matrix. Optimal size-sieving performance for C_3H_6/C_3H_8 separation was exhibited by CMS derived from the ETDA precursor polyamide (ETDA700), with a C_3H_6 uptake value of 2.33 mmol/g, while C_3H_8 molecules were excluded, as confirmed by a single-component adsorption isotherm. The superior performance can be attributed to the ultramicropores, which predominantly fall within the narrow range of 4.8−5.3 Å. Fixed-bed experiments and cyclic regeneration were conducted to evaluate the potential of ETDA700 for practical applications. The work highlights that pore architecture can be manipulated by varying the relative aromatic/aliphatic content of the carbon precursor and efficient size-sieving of small gas molecules can be achieved.

2. EXPERIMENTAL SECTION

2.1. Materials. All the chemicals and reagents including benzene-1,4-diamine (PPDA), ethane-1,2-diamine (ETDA), propane-1,3-diamine (PRDA), 1,3,5-benzenetricarbonyl trichloride (TMC), suberoyl chloride, and *n*-hexane were all used as received without any further purification. CO_2, N_2, C_3H_6, C_3H_8, and deionized water were used for carbonization, physical activation, and adsorption−desorption measurements.

2.2. Synthesis of Polyamide-Derived Carbons. A series of aromatic to fully aliphatic polyamide precursors were synthesized via a well-established interfacial polymerization technique with minor modifications.[16] Typically, diamine monomers (11.3 mmol each) and 1,3,5-benzenetricarbonyl trichloride or suberoyl chloride (7.53 mmol) were concurrently dissolved in deionized water (200 mL) and *n*-hexane (200 mL), respectively, to prepare separate aqueous and organic solutions. These aqueous and organic solution pairs were then combined and magnetically stirred to enhance the interfacial area, ensuring the completion of polyamide formation. The resultant polyamides were then removed from the reaction medium and dried at 100 °C overnight to ensure complete evaporation of any residual *n*-hexane or water. Following this, the dried polyamides were rinsed with water and ethanol several times, aimed at removing any unreacted monomers, and re-dried. For carbonization, the polyamides were then placed in a ceramic combustion boat and introduced into a three-zone tube furnace, under a nitrogen atmosphere, programmed at a ramp rate of 5 °C/min until it reached 700 °C and maintained for

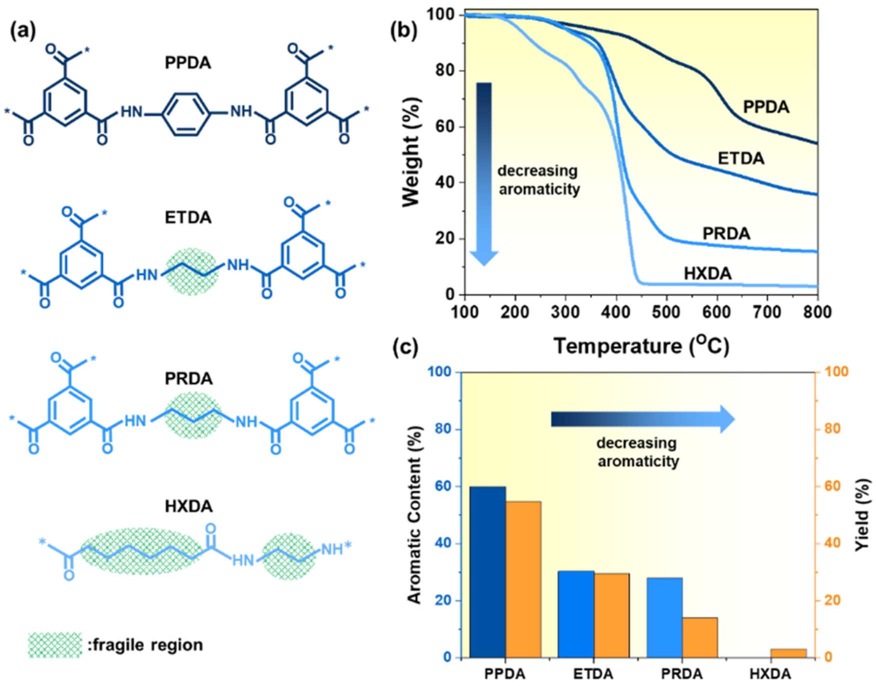

Figure 2. (a) Simplified schematic illustration of chemical structures emphasizing the less stable aliphatic regions in different polyamides, (b) TG weight loss curves measured at 10 °C/min under N_2 flow, and (c) the relationship between aromatic content vs yield of precursor materials.

90 min. After they were cooled, the samples were transferred to storage vials and labeled according to the diamine monomer used and the carbonization temperature. For instance, "PPDA" represented a polyamide derived from benzene-1,4-diamine (*p*-phenylenediamine), while "PPDA700" indicated the corresponding sample carbonized at 700 °C.

2.3. Characterization and Adsorption Measurements.

2.3.1. Material Characterization. Thermogravimetric analysis curves were obtained under nitrogen purge with a heating rate of 10 °C/min to a maximum temperature of 900 °C on a TG55 instrument (TA Instruments, USA). Thermogravimetric mass spectroscopy data were obtained on a Netzsch STA449F3 instrument, which was attached to a Netzsch QMS 403Q (Germany) mass spectrometer. ^{1}H-NMR spectra were measured on a Bruker 400M instrument (with DMSO-d_6 as the solvent). Sample morphology was characterized by scanning electron microscopy (Hitachi S-4800, Hitachi High-Technologies Corporation, Japan) after gold deposition. The samples were analyzed using an X-ray diffractometer (XRD, Bruker D8 ADVANCE, Germany). The surface chemical composition was determined by K-Alpha XPS (Thermo Fisher Scientific, West Palm Beach, FL). Raman spectroscopy was performed with a WITec alpha300R instrument (Germany) with 532 nm laser excitation.

2.3.2. Adsorption Experiments. Adsorption isotherms for C_3H_6 and C_3H_8 at 273, 298, and 313 K and N_2 at 77 K were conducted volumetrically using a Micromeritics 3 FLEX analyzer. The sample (∼100 mg) was degassed at 150 °C under vacuum for at least 5 h before the adsorption measurements. Regeneration ability tests were performed using the same Micromeritics 3 FLEX analyzer as above followed by degassing of the sample at 150 °C under vacuum after each adsorption cycle. CO_2 adsorption isotherms at 273 K using an ASAP 2020 Physisorption analyzer (Micromeritics) were utilized to determine the textural properties of each CMS material. Water adsorption isotherms at 298 K were measured volumetrically using a BELSORP MAX instrument (MicrotracBEL).

2.3.3. Breakthrough Experiments. The dynamic breakthrough experiments were performed on a GC6600 FID analyzer equipped with a stainless-steel column fixed-bed packed with 1 g of adsorbent, and a 50/50 v/v binary gas mixture of C_3H_6/C_3H_8 was used with a flow rate of 2 mL/min. After breakthrough analysis, desorption experiments were conducted by switching the flow gas to Ar and heating the samples to 423 K. Moreover, the C_3H_6 and C_3H_8 dynamic adsorption capacities were calculated according to the following equation:

$$Q = \frac{q}{V_\mathrm{m} \times m} \int_{t_1}^{t_2} (C_\mathrm{o} - C_\mathrm{i})\,\mathrm{d}t$$

where Q is the adsorption capacity (mmol/g), q is the total gas flow rate (mL/min), V_m is the molar volume of the gas (mL/mmol), m is the mass of adsorbents (g), and C_o and C_i are the C_3H_6 or C_3H_8 concentrations at the inlet and outlet, respectively.

2.3.4. Adsorption Enthalpy Calculations. Using the Virial equation, the isosteric heat of adsorption can be estimated from the adsorption isotherms at 273, 298, and 313 K:[17]

$$\ln P = \ln N + 1/T \sum_{i=o}^{m} a_i N_i + \sum_{j=o}^{n} b_j N_j$$

In this equation, P refers to the pressure (bar), N represents the amount absorbed (mmol/g), T is the temperature (K), a_i and b_j are Virial coefficients, and m and n represent the number of coefficients required to adequately describe the isotherms. Also, the values of Virial coefficients a_0 to a_m were then used to calculate the isosteric heat of absorption using the following expression:

$$Q_\mathrm{st} = -R \sum_{i=o}^{m} a_i N_i$$

Here, Q_st represents the coverage-dependent isosteric heat of adsorption and R refers to the ideal gas constant.

3. RESULTS AND DISCUSSION

3.1. Influence of Relative Aromaticity/Aliphaticity on Thermal Degradation Behavior.

Initially, a series of aromatic to fully aliphatic polyamide precursors was prepared via interfacial polyamidation of TMC or suberoyl chloride with different diamines, aimed at adjusting the relative aromaticity and aliphaticity, as shown in Figure 2a. Contrary to other commonly used carbon synthesis strategies,[18] precursor polyamides were obtained through instant interfacial polymer-

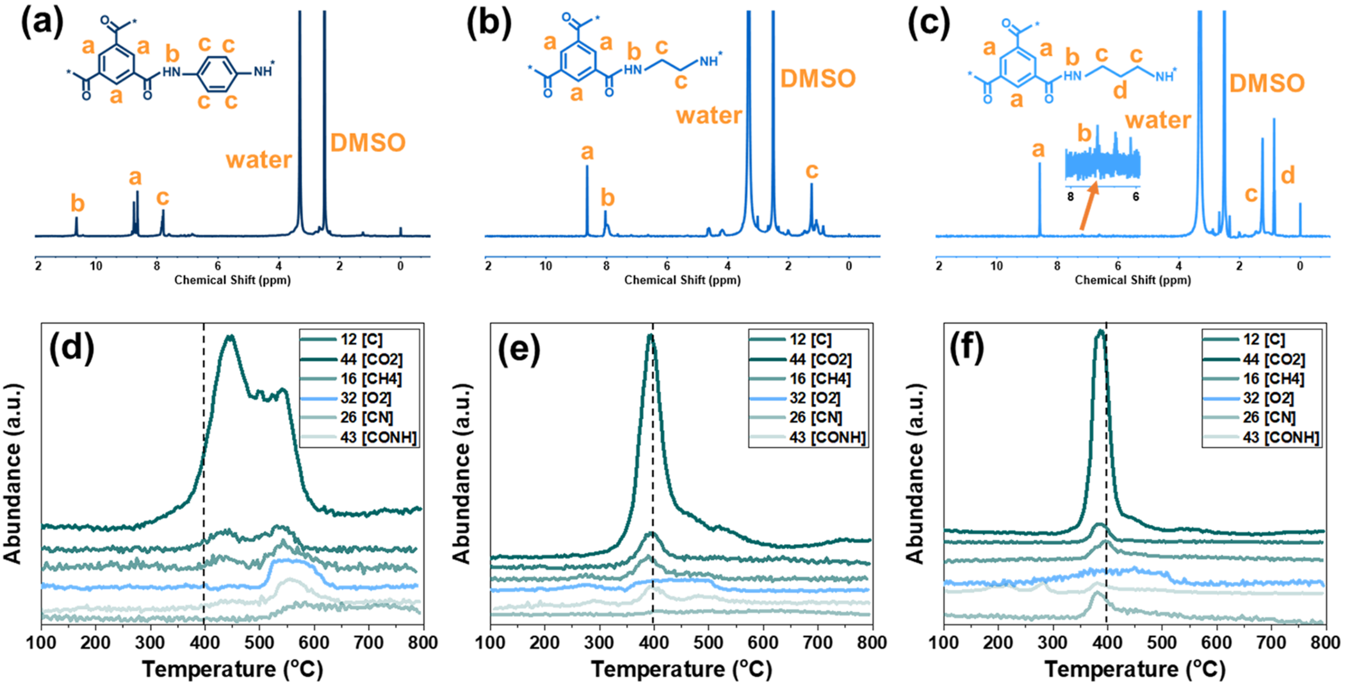

Figure 3. (a−c) ^{1}H NMR spectra and (d−f) TG-MS profiles of PPDA, ETDA, and PRDA precursor polyamides.

ization at ambient conditions and without using any strong organic solvents. Also, the carbonization of polyamides was carried out under inert environments without using any chemical activators, thus eliminating any additional washing and drying steps. Moreover, the hexane−water reaction mixtures were magnetically stirred to enhance the interfacial area and ensure complete polyamidation by mitigating the "self-limiting effect"[19] due to polyamide film thickening.

Thermogravimetric analysis (TGA) was employed to assess the impact of different aromaticity/aliphaticity structures on thermal degradation behavior of the polyamide precursor, as depicted in Figure 2b. TGA profiles revealed that aromatic polyamides, i.e., PPDA, exhibited a greater thermal stability, indicated by the highest residue yield of 54% at 900 °C, while semi-aromatic (ETDA, PPDA) and fully aliphatic polyamides (HXDA) had lower or no yields, highlighting their reduced thermal stability. The enhanced or complete thermal degradation underlines thermal instability of the aliphatic chains, likely influencing the textural properties of carbonized products obtained from semi-aromatic polyamides. Moreover, the TGA curves of semi-aromatic polyamides showed multistage weight loss profiles, with the first zone up to 300 °C induced by moisture desorption and loss of volatile components. The second zone from 300 to 500 °C involved significant structural changes through polyamide backbone degradation. In contrast to the step-wise weight loss profile observed in the aromatic polyamides TG curve, increasing the aliphatic content of the polyamide precursor led to sharp weight loss curves due to the ready breakdown of carbon chains. Above 600 °C, the third zone showed minimal weight reduction, signifying the rearrangement of carbonaceous structures and pore adjustment. Stoichiometric calculations revealed an increased aromatic content, which significantly contributes to the elevated percentage residue yield of polyamides, as shown in Figure 2c.

Moreover, the production yield of carbons was obtained by dividing the weight of the final activated carbon by the initial mass of the precursor polymers. Considering the weight loss incurred by maintaining the temperature at 700 °C, the final yields of all samples were in good agreement with thermogravimetric curves as well as stoichiometric calculations. As shown in Figure S10, the polyamides derived from the PPDA, ETDA, and PRDA precursors produced carbon yields of 43.6%, 18.1%, and 11.61% of the polymer weight, respectively. The above results suggest that relative aromaticity/aliphaticity of the precursor may play a key role on the structural evolution of carbon during carbonization and requires further exploration to elucidate the underlying degradation mechanism. The distinct thermal behaviors of precursors with different relative aromaticity/aliphaticities were further evidenced by comparing SEM images of precursor polyamides and their corresponding carbonized products (Figure S1). The precursor polyamides exhibited a ridge−valley smooth morphology, which is typical for polyamide thin films synthesized through interfacial polymerization.[20] The morphological characteristics underwent a significant transformation upon carbonization at 700 °C. Specifically, the PPDA precursor mainly retained thin film morphology, indicating its greater stability of the polymer matrix, whereas the carbonization of aliphatic polyamides entailed the elimination of less stable carbon chains, resulting in the formation of a more graphitic carbon structure.

Figures 3a−3c present the ^{1}H NMR spectra of PPDA, ETDA, and PRDA precursor polyamides, disclosing the successful interaction between diamine monomers and carbonyl functionalities of TMC through an interfacial polymerization reaction. Notably, the symmetric aromatic protons from TMC, marked as **a**, exhibited a downfield shift in PPDA associated with de-shielding due to the electron-withdrawing effect of delocalized π electrons in the neighboring aromatic rings.[21] In contrast, the presence of fewer electron-withdrawing aliphatic chains with localized electrons resulted in increased shielding; hence, the aromatic protons peak observed a weaker downfield shift in ETDA and PRDA. Additionally, the spatial arrange-

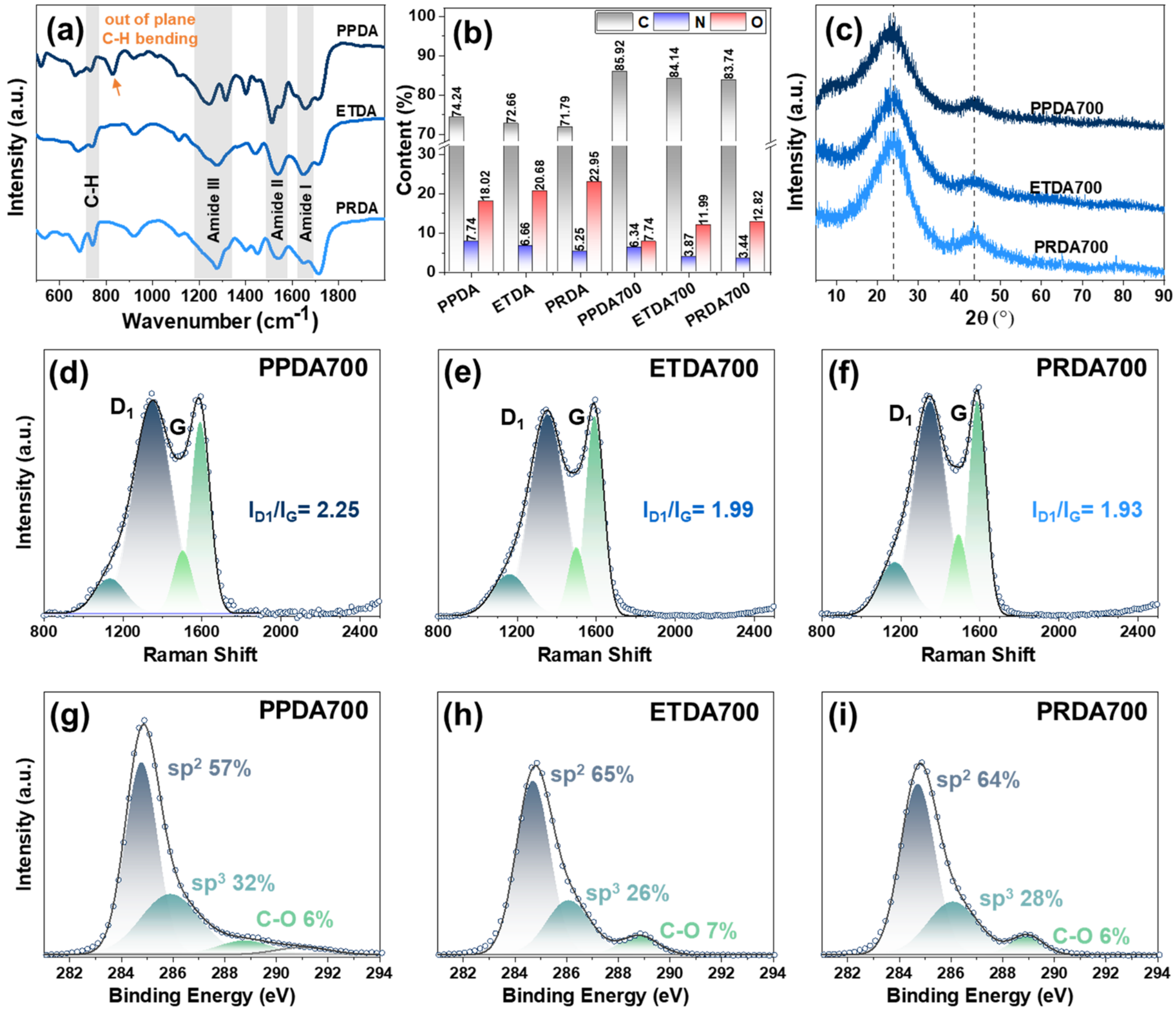

Figure 4. (a) FTIR spectra of precursor polyamides, (b) elemental composition of precursor polyamides and carbonized products as probed by XPS and (c) XRD spectra, and (d–f) deconvoluted Raman and (g–i) high-resolution C 1s spectra of carbonized products.

ment and steric factors of the aliphatic chains, compared to more rigid aromatic rings, influenced the amide protons, denoted as **b**.[22] The NH peaks shifted from 10.6 to 7.9 ppm in the aliphatic variants, which was coupled with a remarkable decrease in the intensity and a broadening of the peaks. Moreover, aromatic/aliphatic protons from diamine moieties indicated relevant peaks in their respective regions, indicating the varying local electronic environments of the carbon atoms. These variations in electronic environments are likely to generate distinct degradation mechanisms, thereby influencing the textural properties of carbonized products.

Thermogravimetric mass spectrometry (TG-MS) was further employed to unveil the degradation mechanisms during carbonization by analyzing effluent gases, as shown in Figures 3d–3f. It can be seen that significant decomposition of all polyamides occurs at around 400 °C. Weight loss occurs in two distinct phases in PPDA at temperatures of 440 and 530 °C. The initial phase involved the release of gasified coke (*m*/*z* 12), carbon dioxide (*m*/*z* 44), and methane (*m*/*z* 16), indicating the simultaneous breakdown and reaction of unstable oxygen and carbon functionalities. In the second phase, the evolution of oxygen (*m*/*z* 32), cyano radicals (*m*/*z* 26), and amide radicals (*m*/*z* 43) coupled with the formation of several higher molecular weight compounds indicates degradation of the polyamide backbone and a series of complex reactions taking place at higher temperature, as indicated by Figure S2. Differently, for aliphatic ETDA and PRDA polyamides, only one sharp peak is observed, characterized by the cleavage of aliphatic chains at a lower temperature of ~400 °C in a single rapid degradation step and rearrangement of polyamide backbones subsequently. The lower degradation temperature observed in aliphatic ETDA and PRDA polyamides can be ascribed to their increased unstable carbon content, which is prone to fragmentation under minimal thermal energy input. The comparative instability of the carbon framework in aliphatic ETDA and PRDA polyamides, in contrast to aromatic PPDA polyamides, was supported by the TG results. Note that the absence of significant water peaks across all polyamides apparently results from the lack of hydroxyl groups in polyamides; rather, traces of methane (*m*/*z* 16) were formed by the reaction of released hydrogens with carbon atoms. According to the TG and TG-MS results, polymers with various relative aromaticity/aliphaticity exhibited differential thermal degradation processes, which were likely a result of varying degrees of restructuring and polycondensation of carbon layers, hence influencing the pore structure of carbonized products.

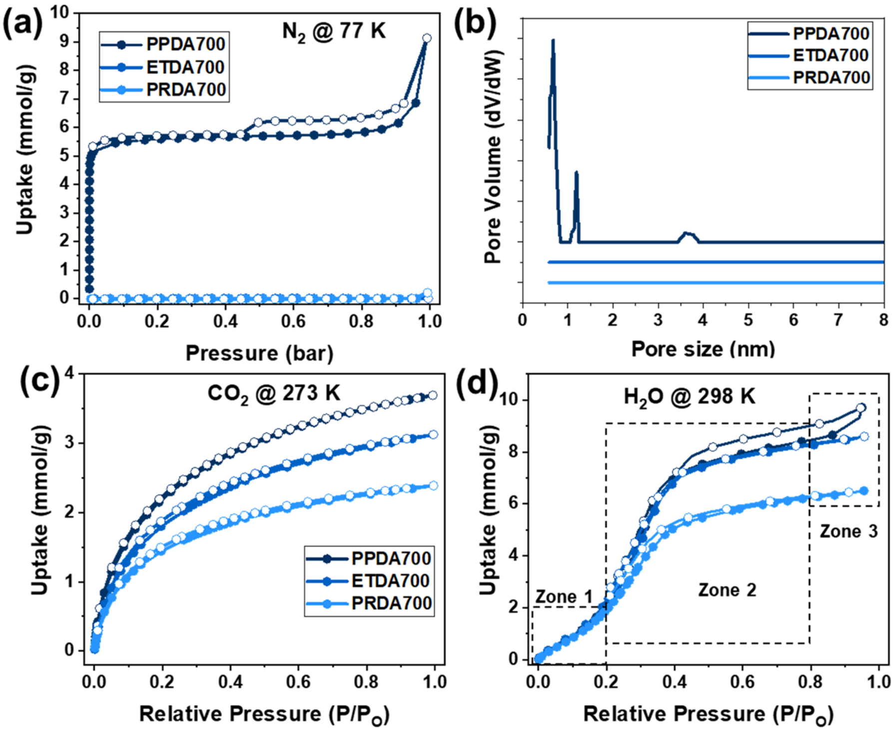

Figure 5. (a) N_2 adsorption−desorption isotherms at 77 K, (b) the pore size distribution of carbonized products obtained from the NLDFT method, (c) CO_2 adsorption−desorption isotherms at 273 K, and (d) water vapor adsorption−desorption isotherms at 298 K.

3.2. Influence of Relative Aromaticity/Aliphaticity on the Structural Characteristics.

Fourier transform infrared (FTIR) spectroscopy was performed to characterize the surface chemistry of the synthesized polyamide precursor, as depicted in Figure 4a. The FTIR spectra prominently featured the characteristic polyamide peaks. The amide I band, typically in the 1630−1690 cm^{-1} range and attributed to the C═O stretching vibrations,[23] reflects consistent conformation across all polyamides. The amide II band located at 1480−1575 cm^{-1} corresponds to the N−H bending and C−N stretching vibrations. Notably, a shift to higher wavenumbers in aliphatic chain-containing polyamides compared to aromatic ones reflects varying electrostatic interactions.[24] The amide III band, within the 1200−1300 cm^{-1} region, displayed a pattern of overlaid peaks from the combined C−N stretching and N−H in-plane bending vibrations depending on the diamine's nature.[25] Moreover, out-of-plane C−H bending vibrations are indicative of aromatic structures, appearing between 600−900 cm^{-1}. A distinct peak near 830 cm^{-1} in the PPDA confirms the aromaticity, while the absence of such ETDA and PRDA counterparts highlights their aliphatic character. Surface elemental composition of precursors and carbonized products was investigated through XPS. The precursor polyamides show a significant nitrogen and oxygen content. Upon carbonization, the oxygen content decreases from ∼20% to ∼10% across all polyamides, reflecting the scission of more volatile carbonyl functionalities. On the other hand, loss in nitrogen content is less obvious for PPDA in comparison to ETDA and PRDA, indicating the presence of stable amines attached with aromatic rings. This structural evolution was further characterized by XRD, as shown in Figure. 4c, and D spacing (D_{002}) was calculated using Bragg's equation and the Origin peak analysis tool. Interestingly, diffraction peaks (2θ) and subsequently D_{002} values for all carbonized products were in a close range around ∼25° and 3.9 Å, respectively. Proximate 2θ values suggest that carbon layer spacing is more of a temperature-regulated phenomenon and pore diameter is mainly steered by the defects within carbon layers, which can be tuned by changing the chemical structure of the precursor material.

Additionally, Raman spectroscopy analysis was performed to explain the influence of increasing relative aliphaticity on the content of defects (Figures 4d−4f). Two prominent peaks, characteristic of amorphous carbons, were deconvoluted using a four-band model, where the G band near 1590 cm^{-1} indicates the presence of graphitic domains while the D band around 1350 cm^{-1} signifies defects or disorder within the carbon lattice.[26] The intensity ratio I_{D1}/I_G, a significant indicator of the degree of graphitization, decreased from 2.25 in PPDA700 to 1.93 in PRDA700, indicating a higher degree of graphitization with fewer defects. Higher aromatic content in the polymer matrix preserved the polyamide's original structure with decreased graphitization. To verify the trend observed in Raman spectroscopy, X-ray photoelectron spectroscopy (XPS) spectra were obtained. The relative content of sp^2/sp^3 hybridized carbons was estimated from the deconvoluted C 1s peak areas, as depicted in Figures 4g−4i. The relative sp^2 peak area increased from 57% to 65%, confirming the role of aliphatic carbon-chain-containing diamines in increased graphitization.[27] Henceforth, it is reasonable to infer that increased relative aliphaticity in polyamide precursors can effectively eliminate the unstable carbon chains upon the carbonization process, leading to the formation of a more graphitic carbonaceous structure through a higher degree of carbon structure rearrangement.

The increased relative aliphaticity in precursor polyamides results in a more ordered graphitic structure, which favors the creation of smaller structural voids within the carbon matrix. Therefore, the textural properties of carbonized samples were

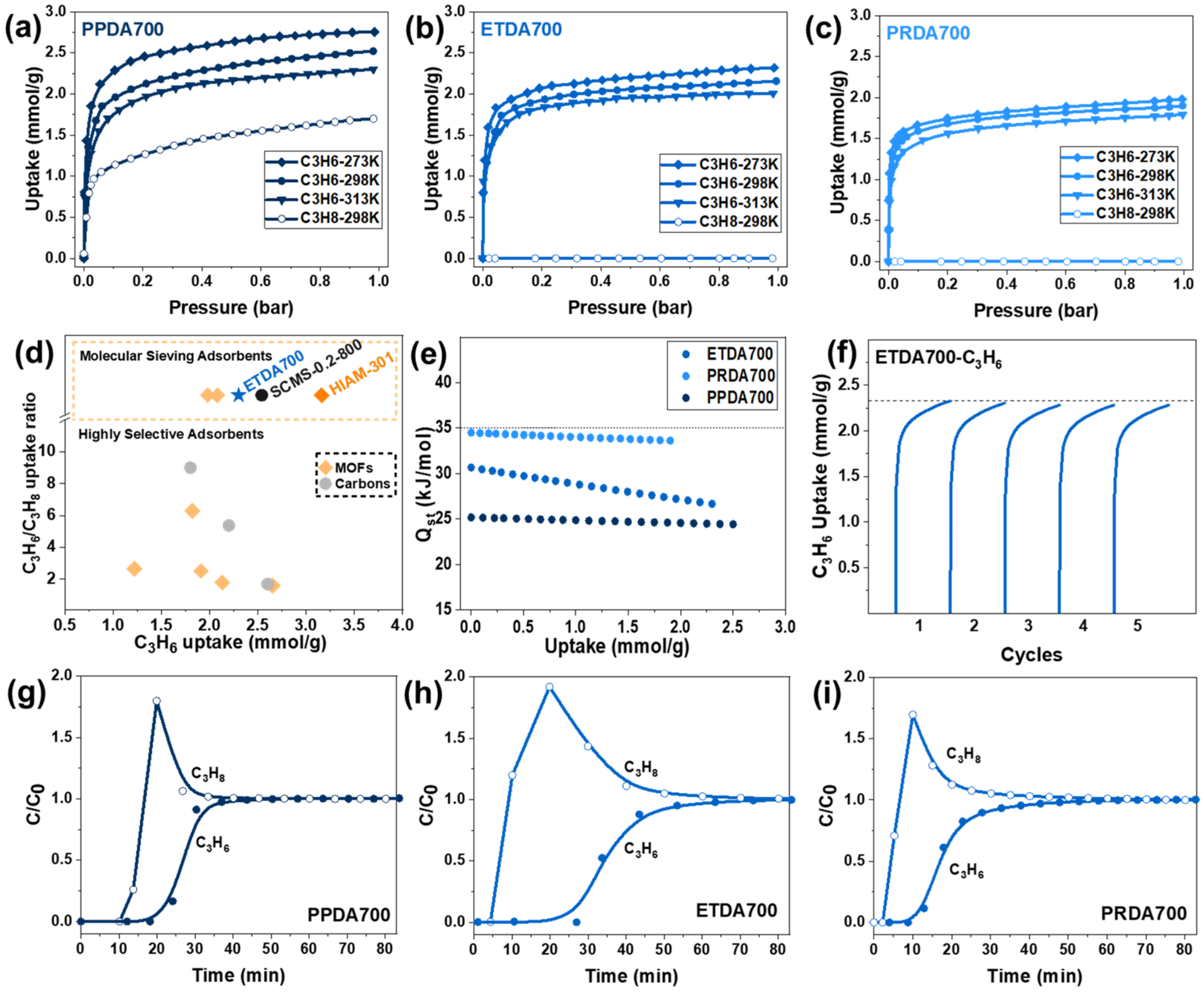

Figure 6. (a–c) Single-component C_3H_6 and C_3H_8 adsorption isotherms of CMS adsorbents at 298 K, (d) comparison of C_3H_6 uptake vs C_3H_6/C_3H_8 uptake ratio for different carbon adsorbents reported in the literature, (e) adsorption enthalpies of carbonized products for C_3H_6 molecules, (f) cycling C_3H_6 adsorption performance of ETDA700, and (g–i) experimental breakthrough curves of PPDA700, ETDA700, and PRDA700 for separating equimolar volume ratios of a C_3H_6/C_3H_8 mixture at 298 K and 1.0 bar.

evaluated using N_2 and CO_2 as probe gases. PPDA700 exhibited a type IV isotherm profile, characterized by a hysteresis loop (according to the IUPAC classification[28]), with N_2 uptake of 9.13 mmol/g at 77 K, indicating the presence of micro- and mesopores (Figure 5a). The calculated pore size based on the nonlinear density functional theory (NLDFT) model is centered at 0.67, 1.19, and 3.7 nm (Figure 5b). Contrarily, ETDA700 and PRDA700 showed almost no N_2 adsorption (<0.01 mmol g^{-1}), suggesting the absence of pores above 5.0 Å.[29] Nevertheless, the remarkable adsorption capacity of CO_2 over ETDA700 and PRDA700 at 273 K (Figure 5c) indicated the presence of ultramicropores, which were undetected by N_2 molecules due to kinetic restrictions at 77 K. Based on the DFT model, a same pore size distribution (PSD) centered at 3.5 and 4.8 Å was observed for PPDA700, ETDA700, and PRDA700 (Figure S3). Notably, the PSD within the micropore scale precisely lies between the kinetic diameters of C_3H_6 (4.68 Å) and C_3H_8 (5.11 Å); thus, it can be reasonably inferred that ETDA700 and PRDA700 are potential size-sieving adsorbents for C_3H_6/C_3H_8 separation. The discrepancy in pore size distribution between PPDA700 and aliphatic carbon-chain-containing polyamide-derived CMS (ETDA700 and PRDA700) was rationalized by the greater extent of structure rearrangement resulting from the increased aliphaticity of the precursor. Water vapor adsorption isotherms at 298 K were then measured to further verify the porous structure and surface chemistry of carbonized products. The low water uptake (<2 mmol/g) in zone 1 (P/P_0 < 0.3) demonstrates the hydrophobic character of carbon surfaces, while gradually increased uptake in zone 2 ($0.3 < P/P_0 < 0.8$) exhibits the filling of narrow ultramicropores. Also, a slower accumulation of water vapors into the PRDA700 ultramicropores suggested rather restricted diffusion and smaller specific surface area, which is also evident from N_2 and CO_2 isotherms. In zone 3 (P/P_0 > 0.8), the obvious hysteresis loop due to capillary condensation further confirms the presence of mesopores in PPDA700. The above results reveal that ETDA700 and PRDA700 possess smaller ultramicropores, allowing smaller CO_2 molecules (3.3 Å) to pass through while rejecting N_2 (3.64 Å) molecules. The accessible pores within aliphatic carbon-chain-containing polyamide-derived carbons are centered around 4.8 Å, which is essential for the efficient sieving of C_3H_6 from C_3H_8.

3.3. C_3H_6/C_3H_8 Adsorption Separation Performance.

Considering the presence of narrowly distributed ultramicropores in ETDA700 and PRDA700, single-component gas adsorption isotherms for C_3H_6 and C_3H_8 were measured to evaluate their potential in selective gas-phase separation, as depicted in Figures 6a−6c. Due to the higher surface area contributed to by mesopores, the PPDA700 sample exhibited the highest C_3H_6 adsorption capacity (2.52 mmol/g) but poor selectivity with an uptake ratio of 1.48 because the widely distributed ultramicropores are larger than the C_3H_8 molecules and unable to exhibit the size-sieving effect. Contrarily, CMS derived from the ETDA and PRDA precursors displayed remarkable C_3H_6/C_3H_8 separation performance due to their narrowly distributed sub 5 Å pores capable of rejecting C_3H_8 molecules. As shown in Figures 6b and 6c, the isotherms of C_3H_6 and C_3H_8 showed significant divergence for ETDA700 and PRDA700. ETDA700 and PRDA700 had adsorption uptakes of 2.33 and 1.89 mmol/g for C_3H_6, respectively, while both showed negligible adsorption of C_3H_8, confirming the efficient size-sieving of C_3H_6 from C_3H_8. The excellent separation performance was attributed to the ultramicropore size that lies between the kinetic diameters of C_3H_6 and C_3H_8, resulting in the complete exclusion of C_3H_8. Despite the size-sieving performance for both ETDA700 and PRDA700, ETDA700 exhibited higher adsorption capacity for C_3H_6, owing to their higher cumulative pore volume as calculated by CO_2 adsorption isotherms. Note that neither of the precursor polyamides exhibited adsorption of C_3H_6 or C_3H_8 (Figure S3), indicating that the induction of porosity occurs solely during carbonization at high temperature. Moreover, kinetic adsorption experiments of C_3H_6 and C_3H_8 were conducted on CMS samples, as depicted in Figure S8. The results were consistent with static adsorption isotherms, where PPDA700 and PRDA700 struggled with poor selectivity and slower kinetics, respectively. Meanwhile, ETDA700 exhibited promising performance with excellent selectivity and relatively faster kinetics for C_3H_6 adsorption. These adsorption experiments, supplemented by structural and morphological analyses, verified that the selectivity and capacity of polyamide-derived carbon sorbents can be tuned by varying the relative aliphatic content of distinct diamine monomers for interfacial polymerization.

Further, the C_3H_6 uptake capacities of the synthesized sorbents were compared with those of other benchmark sorbents reported in the literature at 100 KPa and 298 K (Figure 6d). Among the tested sorbents, C_3H_6 adsorption capacity and uptake ratio are significantly greater than those of most of the other reported carbons and crystalline MOFs. Also, the isosteric heat of adsorption (Q_{st}) is a crucial parameter for evaluating the strength of adsorbate−adsorbent interactions and potential regeneration requirements. In this study, the Q_{st} values were calculated using virial equations for adsorption isotherms measured at three different temperatures. The Q_{st} values for C_3H_6 were found in physisorption range (1−40 kJ/mol),[30] indicating an easy regeneration, which was further validated by five adsorption−desorption cycles of ETDA700 with only a minimal 2.5% decrease in adsorption uptake. Column breakthrough experiments were conducted to evaluate the separation performance of realistic gas mixtures. Using C_3H_6/C_3H_8 at 298 K and 1 bar, the adsorption column packed with 1 g of ETDA700 materials efficiently separated C_3H_8 within 1 min while retaining C_3H_6 for over 20 min (Figures 6g−6i). Additionally, the dynamic adsorption capacity for CMS samples was also calculated, where PPDA700 and ETDA700 exhibited a cumulative uptake of 1.79 and 1.75 mmol/g, respectively, while PRDA had an uptake of only 0.91 mmol/g, which may be attributed to diffusion limitations as evidenced by kinetic curves. Furthermore, desorption curves of ETDA700 were obtained by heating the samples to 403 K and the results indicated that >99 % purity of C_3H_6 can be achieved. This remarkable elution time difference along with the high purity of C_3H_6 highlights the promising separation efficiency of ETDA700 for C_3H_6/C_3H_8 under practical conditions.

4. CONCLUSION

In conclusion, we report a strategy by regulating the relative aliphaticity/aromaticity of the polyamide precursor for the control of ultramicropore pore size in derived carbon to be within sub 5 Å. The rules governing the adjustment of pore size distribution based on the relative aliphaticity/aromaticity of the precursor were investigated systematically. The results conclusively show that the carbonization of aliphatic polyamides effectively eliminates unstable carbon chains, leading to the formation of a more graphitic carbonaceous structure through varying degrees of melt polycondensation. Consequently, this process favors the shrinkage of the pores to a smaller size. The obtained ETDA700 materials exhibited a superior size-sieving effect for C_3H_6/C_3H_8 and 2.33 mmol/g uptake for C_3H_6, while PPDA700 and PRDA700 struggled with poor selectivity and lower C_3H_6 uptake, respectively. Breakthrough experiments confirmed the superior C_3H_6/C_3H_8 dynamic separation performance of the ETDA700 materials. This study provides insights in designing carbon materials with well-controlled porous structures for the molecular sieving of light hydrocarbon pairs.

■ ASSOCIATED CONTENT

Supporting Information

The Supporting Information is available free of charge at https://pubs.acs.org/doi/10.1021/cbe.4c00095.

> SEM images of precursors and corresponding carbonized products, TG-MS profiles, pore size distribution obtained from CO_2 isotherms, single-component adsorption isotherms, single-component kinetic curves, desorption curves, production yield of carbonized products, self-assembly breakthrough experimental setup, comparison table of different adsorbent materials, and table of isosteric heats of adsorption fitting parameters (PDF)

■ AUTHOR INFORMATION

Corresponding Authors

Cuiting Yang − *School of Chemistry and Chemical Engineering, South China University of Technology, Guangzhou 510640, P. R. China*; Email: cuitingyang@scut.edu.cn

Jing Xiao − *School of Chemistry and Chemical Engineering, South China University of Technology, Guangzhou 510640, P. R. China*; orcid.org/0000-0002-7006-6211; Email: cejingxiao@scut.edu.cn

Authors

Abdul Waqas Anjum − *School of Chemistry and Chemical Engineering, South China University of Technology, Guangzhou 510640, P. R. China*

Lin Zhu − *School of Chemistry and Chemical Engineering, South China University of Technology, Guangzhou 510640, P. R. China*
Jiawu Huang − *School of Chemistry and Chemical Engineering, South China University of Technology, Guangzhou 510640, P. R. China*
Neng Liao − *School of Chemistry and Chemical Engineering, South China University of Technology, Guangzhou 510640, P. R. China*
Shengjun Du − *School of Chemistry and Chemical Engineering, South China University of Technology, Guangzhou 510640, P. R. China*
Zhong Li − *School of Chemistry and Chemical Engineering, South China University of Technology, Guangzhou 510640, P. R. China;* orcid.org/0000-0002-2796-9300

Complete contact information is available at:
https://pubs.acs.org/10.1021/cbe.4c00095

Notes

The authors declare no competing financial interest.

■ ACKNOWLEDGMENTS

We gratefully acknowledge the support from the National Natural Science Foundation of China (22278146, 22308106, and 21978099) and the Guangdong Natural Science Foundation (2023A0505010002).

■ REFERENCES

(1) Phung, T. K.; Pham, T. L. M.; Vu, K. B.; Busca, G. (Bio)Propylene production processes: A critical review. *Journal of Environmental Chemical Engineering* **2021**, *9* (4), No. 105673.

(2) Martins, V. F. D.; Ribeiro, A. M.; Plaza, M. G.; Santos, J. C.; Loureiro, J. M.; Ferreira, A. F. P.; Rodrigues, A. E. Gas-phase simulated moving bed: Propane/propylene separation on 13X zeolite. *Journal of Chromatography A* **2015**, *1423*, 136−148.

(3) Xu, Y.; Zuo, Y.; Yang, W.; Shu, X.; Chen, W.; Zheng, A. Targeted Catalytic Cracking to Olefins (TCO): Reaction Mechanism, Production Scheme, and Process Perspectives. *Engineering* **2023**, *30*, 100−109.

(4) Du, S.; Huang, B.; Zhu, L.; Wu, Y.; Huang, J.; Li, Z.; Yu, H.; Xiao, J. Optimizing gas transport for C3H6/C3H8 size sieving separation via fine pore engineering of carbon microspheres. *Carbon* **2023**, *215*, No. 118451.

(5) Eldridge, R. B. Olefin/paraffin separation technology: a review. *Industrial & Engineering Chemistry Research* **1993**, *32* (10), 2208−2212.

(6) Selmert, V.; Kretzschmar, A.; Weinrich, H.; Tempel, H.; Kungl, H.; Eichel, R.-A. CO2/N2 Separation on Highly Selective Carbon Nanofibers Investigated by Dynamic Gas Adsorption. *ChemSusChem* **2022**, *15* (14), No. e202200761.

(7) Rocha, L. A. M.; Andreassen, K. A.; Grande, C. A. Separation of CO2/CH4 using carbon molecular sieve (CMS) at low and high pressure. *Chemical Engineering Science* **2017**, *164*, 148−157.

(8) Du, S.; Wu, Y.; Wang, X.; Xia, Q.; Xiao, J.; Zhou, X.; Li, Z. Facile synthesis of ultramicroporous carbon adsorbents with ultra-high CH4 uptake by in situ ionic activation. *AIChE Journal* **2020**, *66* (7), No. e16231.

(9) Huang, B.; Zhu, L.; Du, Z.; Anjum, A. W.; Li, X.; Li, X.; Miao, G.; Xiao, J.; Du, S. Highly efficient ethylene/ethane separation via molecular sieving using chitosan-derived ultramicroporous carbon. *Sep. Purif. Technol.* **2024**, *333*, No. 125862.

(10) Du, S.; Huang, B.; Hao, G. P.; Huang, J.; Liu, Z.; Oschatz, M.; Xiao, J.; Lu, A. H. pH-Regulated Refinement of Pore Size in Carbon Spheres for Size-Sieving of Gaseous C8, C6 and C3 Hydrocarbon Pairs. *ChemSusChem* **2023**, *16* (16), No. e202300215.

(11) Perovic, M.; Qin, Q.; Oschatz, M. From Molecular Precursors to Nanoparticles—Tailoring the Adsorption Properties of Porous Carbon Materials by Controlled Chemical Functionalization. *Adv. Funct. Mater.* **2020**, *30* (41), No. 1908371.

(12) Babu, D. J.; Bruns, M.; Schneider, R.; Gerthsen, D.; Schneider, J. J. Understanding the Influence of N-Doping on the CO2 Adsorption Characteristics in Carbon Nanomaterials. *J. Phys. Chem. C* **2017**, *121* (1), 616−626.

(13) Rahimi, V.; Ferreiro-Salgado, A.; Gómez-Díaz, D.; Freire, M. S.; González-Álvarez, J. Evaluating the performance of carbon-based adsorbents fabricated from renewable biomass precursors for post-combustion CO_2 capture. *Separation and Purification Technology* **2024**, *344*, 127110.

(14) Kiyono, M.; Williams, P. J.; Koros, W. J. Effect of polymer precursors on carbon molecular sieve structure and separation performance properties. *Carbon* **2010**, *48* (15), 4432−4441.

(15) Solà, M. Aromaticity rules. *Nat. Chem.* **2022**, *14* (6), 585−590.

(16) White, H. D.; Li, C.; Lively, R. P. Tailoring the Structure of Carbon Molecular Sieves Derived from an Aromatic Polyamide. *Industrial & Engineering Chemistry Research* **2022**, *61* (15), 5314−5323.

(17) Li, L.; Lin, R.-B.; Krishna, R.; Li, H.; Xiang, S.; Wu, H.; Li, J.; Zhou, W.; Chen, B. Ethane/ethylene separation in a metal-organic framework with iron-peroxo sites. *Science* **2018**, *362* (6413), 443.

(18) Fan, Q.; Song, C.; Fu, P. Advances in the improvement of the quality and efficiency of biomass-derived porous carbon: A comprehensive review on synthesis strategies and heteroatom doping effects. *Journal of Cleaner Production* **2024**, *452*, No. 142169.

(19) Liu, C.; Yang, J.; Guo, B.-B.; Agarwal, S.; Greiner, A.; Xu, Z.-K. Interfacial Polymerization at the Alkane/Ionic Liquid Interface. *Angew. Chem., Int. Ed.* **2021**, *60* (26), 14636−14643.

(20) Li, L.; Zhang, S.; Zhang, X.; Zheng, G. Polyamide thin film composite membranes prepared from 3,4′,5-biphenyl triacyl chloride, 3,3′,5,5′-biphenyl tetraacyl chloride and m-phenylenediamine. *Journal of Membrane Science* **2007**, *289* (1), 258−267.

(21) Baranac-Stojanović, M. Can Variations of 1H NMR Chemical Shifts in Benzene Substituted with an Electron-Accepting (NO2)/Donating (NH2) Group be Explained in Terms of Resonance Effects of Substituents? *Chemistry − An Asian Journal* **2018**, *13* (7), 877−881.

(22) Zhang, D.-W.; Zhao, X.; Hou, J.-L.; Li, Z.-T. Aromatic Amide Foldamers: Structures, Properties, and Functions. *Chem. Rev.* **2012**, *112* (10), 5271−5316.

(23) Ji, Y.; Yang, X.; Ji, Z.; Zhu, L.; Ma, N.; Chen, D.; Jia, X.; Tang, J.; Cao, Y. DFT-Calculated IR Spectrum Amide I, II, and III Band Contributions of N-Methylacetamide Fine Components. *ACS Omega* **2020**, *5* (15), 8572−8578.

(24) Milani, A.; Castiglioni, C.; Di Dedda, E.; Radice, S.; Canil, G.; Di Meo, A.; Picozzi, R.; Tonelli, C. Hydrogen bonding effects in perfluorinated polyamides: An investigation based on infrared spectroscopy and density functional theory calculations. *Polymer* **2010**, *51* (12), 2597−2610.

(25) Stani, C.; Vaccari, L.; Mitri, E.; Birarda, G. FTIR investigation of the secondary structure of type I collagen: New insight into the amide III band. *Spectrochimica Acta Part A: Molecular and Biomolecular Spectroscopy* **2020**, *229*, No. 118006.

(26) Cuesta, A.; Dhamelincourt, P.; Laureyns, J.; Martínez-Alonso, A.; Tascón, J. M. D. Raman microprobe studies on carbon materials. *Carbon* **1994**, *32* (8), 1523−1532.

(27) Kabir, H.; Zhu, H.; May, J.; Hamal, K.; Kan, Y.; Williams, T.; Echeverria, E.; McIlroy, D. N.; Estrada, D.; Davis, P. H.; Pandhi, T.; Yocham, K.; Higginbotham, K.; Clearfield, A.; Cheng, I. F. The sp2-sp3 carbon hybridization content of nanocrystalline graphite from pyrolyzed vegetable oil, comparison of electrochemistry and physical properties with other carbon forms and allotropes. *Carbon* **2019**, *144*, 831−840.

(28) Thommes, M.; Kaneko, K.; Neimark, A. V.; Olivier, J. P.; Rodriguez-Reinoso, F.; Rouquerol, J.; Sing, K. S. W. Physisorption of gases, with special reference to the evaluation of surface area and pore

size distribution (IUPAC Technical Report). *Pure and Applied Chemistry* **2015**, *87* (9-10), 1051−1069.

(29) Du, S.; Huang, J.; Ryder, M. R.; Daemen, L. L.; Yang, C.; Zhang, H.; Yin, P.; Lai, Y.; Xiao, J.; Dai, S.; Chen, B. Probing sub-5 Ångstrom micropores in carbon for precise light olefin/paraffin separation. *Nat. Commun.* **2023**, *14* (1), 1197.

(30) Egbosiuba, T. C.; Abdulkareem, A. S.; Kovo, A. S.; Afolabi, E. A.; Tijani, J. O.; Auta, M.; Roos, W. D. Ultrasonic enhanced adsorption of methylene blue onto the optimized surface area of activated carbon: Adsorption isotherm, kinetics and thermodynamics. *Chemical Engineering Research and Design* **2020**, *153*, 315−336.